J. Physiol. (1979), **290**, *pp.* 201–225
With 12 *text-figures*
Printed in Great Britain

THREE-MICRO-ELECTRODE VOLTAGE CLAMP EXPERIMENTS IN CALF CARDIAC PURKINJE FIBRES: IS SLOW INWARD CURRENT ADEQUATELY MEASURED?

R. S. KASS*, S. A. SIEGELBAUM† AND R. W. TSIEN

From the Department of Physiology, Yale University School of Medicine, 333 Cedar Street, New Haven, Connecticut 06510, U.S.A.

(*Received 27 September 1978*)

SUMMARY

1. The three-micro-electrode voltage clamp method (Adrian, Chandler & Hodgkin, 1970) was adapted for the study of regenerative inward currents in cardiac muscle. The adequacy of measurements of slow inward current in cardiac Purkinje fibres was assessed.

2. Membrane current density is reported simultaneously by total applied current (I_T), along with a longitudinal voltage difference signal (ΔV), recorded between two intracellular micro-electrodes.

3. Non-linear cable calculations show that ΔV is a more faithful measure of membrane current density than I_T as peak inward current increases. Quantitative agreement between ΔV and I_T only occurs when both signals report the membrane characteristics that would be obtained with an ideal longitudinal space clamp.

4. Agreement between ΔV and I_T is thus a useful criterion for satisfactory experimental measurements which we applied to the slow inward current. This component was elicited by depolarizing steps from a holding potential near -45 mV in the presence of tetrodotoxin. The I_T signal was compared directly with $\Delta V/R$, where R is an effective longitudinal resistance that was experimentally determined.

5. $\Delta V/R$ and I_T showed very good agreement in both peak amplitude and time course at all potentials studied.

6. Radial non-uniformity during the measured peak slow inward current was estimated by calculations assuming clefts 200 Å wide with a uniform distribution of ionic channels. The calculated voltage span from surface to centre was always less than 5 mV, and the measured $I-V$ characteristics showed little distortion.

7. In another check, $I-V$ characteristics and slow response membrane action potentials were compared. The measured peak current showed good agreement with the product (total preparation capacitance) × (rate of rise).

8. The experimental and theoretical analysis suggest that the measurements of slow inward current are a good approximation to genuine membrane properties.

* Present address: Department of Physiology, University of Rochester School of Medicine and Dentistry, Rochester, N.Y. 14602, U.S.A.

† Present address: Department of Pharmacology, St. George's Hospital Medical School, London SW17 0QT.

0022-3751/79/3070-0765 $01.50

INTRODUCTION

Since 1964 considerable effort has been aimed at characterizing the ionic currents of cardiac membranes (Trautwein, 1973; Noble, 1975). There is general agreement that, in principle, voltage clamp experiments in heart can provide valuable information on events underlying excitation and contraction (see for example Reuter, 1974; Fozzard & Beeler, 1975). Much controversy remains, however, concerning the validity of experimental methods presently in use (Johnson & Lieberman, 1971; Tarr & Trank, 1974; Connor, Barr & Jakobsson, 1975; Attwell & Cohen, 1977). Since cardiac preparations cannot be space-clamped with an internal longitudinal electrode, some spatial and temporal non-uniformity must exist. The main issue is one of degree: how serious is the non-uniformity and how faithfully do the recorded currents reflect genuine membrane properties? Questions about the reliability of existing methods lead to several lines of approach: (1) to improve voltage clamp measurements by developing better preparations or better methods for measuring membrane current; (2) to clarify the limitations of various techniques by theoretical modelling; (3) to develop objective criteria for accepting or rejecting experimental information. These goals provide the motivation for this article and a companion paper (Colatsky & Tsien, 1979).

This paper describes an adaptation of the three-micro-electrode method of Adrian *et al.* (1970) for the study of regenerative inward currents. As applied to cardiac preparations, the method employs two independent signals to report membrane current density, a voltage difference signal (ΔV), along with total applied current (I_T). Quantitative agreement between ΔV and I_T can be assessed without arbitrary scaling, and provides a stringent test for acceptable measurements. This approach was applied to the slow inward current, a component essential to the normal action potential plateau and to the activation of contraction (Reuter, 1973). We investigated the degree of voltage non-uniformity during measurements of slow inward current in cardiac Purkinje fibres from calf hearts. Our analysis indicated that non-uniformities were acceptably small, both in the longitudinal direction and radially, along narrow intercellular clefts. Observed values of peak slow inward current were consistent with the rate of rise of regenerative activity ('slow responses'), recorded in the same preparation in the absence of rapid Na current. These considerations show that our measurements of slow inward current are a close approximation to genuine membrane properties.

Preliminary communications of some of this work have been presented to the Biophysical Society (Kass & Tsien, 1975; Kass, Siegelbaum & Tsien, 1978).

METHODS

Experimental procedure

Isolated Purkinje fibre bundles ranging from 1·5 to 2·5 mm in length and 100–200 μm in diameter were excised from either ventricle of calf hearts. Three micro-electrodes were inserted into the preparation as shown in Fig. 1*B*. A current-passing micro-electrode (I_T) filled with 1·5 M-K citrate was placed midway, at a distance h from either end. The total applied current was collected by an Ag-AgCl pellet electrode and measured by a virtual ground amplifier. Two voltage-recording micro-electrodes, each filled with 3 M-KCl, were inserted toward one end;

l is the distance from the end of the preparation to V_1, and αl is the spacing between V_1 and V_2. In general, the spacing ratio α was greater than unity (see Theory). Capacitative coupling to the current-passing micro-electrode was reduced by a grounded metal shield between I_T and V_2. Further shielding was provided in most experiments by coating all three micro-electrodes with a layer of conducting silver paint and a layer of insulating nail polish. The shielding of each voltage electrode was driven by the output of its unity-gain electrometer, and the current-passing electrode shield was grounded.

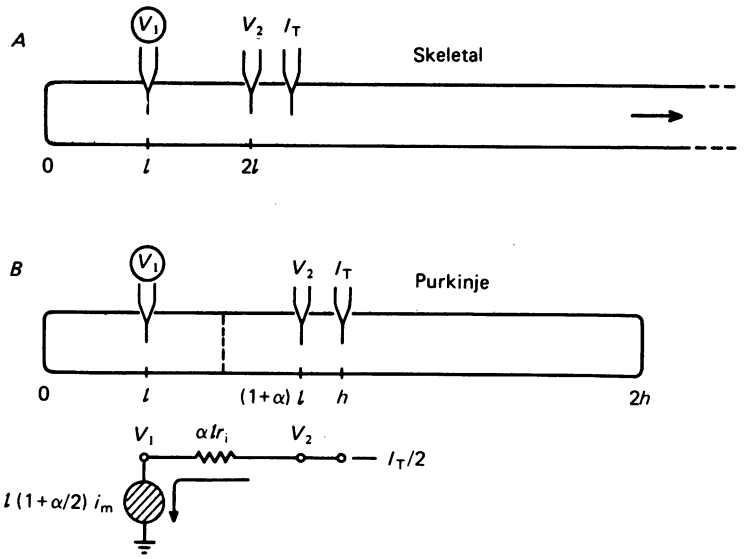

Fig. 1. The three-micro-electrode voltage clamp. *A*, the method originally used in skeletal muscle by Adrian *et al.* (1970). Voltage control is imposed at V_1 and membrane current density is reported by $(V_2 - V_1)$. Total applied current (I_T) is not easily interpretable because of unequal current flow into the short and long ends of the fibre. *B*, the technique adapted for regenerative inward currents in Purkinje fibres. Current-passing electrode is located at a distance h from each sealed end so I_T becomes interpretable. Spacing αl between V_2 and V_1 is adjusted to improve accuracy of $(V_2 - V_1)$ for negative membrane conductance. Optimal spacing for linear case ($\alpha = 1{\cdot}5$) is shown. The $(V_2 - V_1)$ signal approximates i_m over a region from the sealed end to the dashed line. This trans-membrane current flow is indicated by the shaded element in the lumped equivalent circuit below.

The potential difference between the V_1 micro-electrode and bath was controlled by a conventional voltage clamp circuit. Command pulses were rounded with an exponential time constant of 100–300 μsec. This procedure allowed higher clamp gain without ringing of the capacity transient and minimized damage due to large surges of applied current. The voltage difference signal $\Delta V \equiv (V_2 - V_1)$ was taken with a differential amplifier and recorded along with V_1 and I_T on a Brush 440 chart recorder (Gould Inc., Cleveland). The frequency response of the chart recorder was down 3 db at 125 Hz. Records of rapid transients were taken on a 5301 storage oscilloscope (Tektronix, Beaverton, Oregon) or a PDP 8/e digital computer (Digital Equipment Corp., Maynard, Massachusetts).

The Purkinje bundles were incubated and impaled in solution A (Table 1) at 35–37 °C. After penetration by all three micro-electrodes, the superfusate was changed to a solution (B or C) which favoured 'slow responses'. Tetrodotoxin was included to inhibit the fast Na current, I_{Na}. In solution B, I_{Na} was also partially inactivated by depolarizing the membrane to about -60 mV with 16 mM-K. The slow inward current was sometimes enhanced by adding epinephrine bitartrate (10 μM) to solution B. In solution C, Sr was used as a replacement for Ca because

this ion enhances the slow inward current (Vereecke & Carmeliet, 1971) and minimizes interference from calcium-activated transient outward current (Siegelbaum, Tsien & Kass, 1977; Siegelbaum, 1978). In the presence of solutions B or C, slow responses were readily evoked by depolarizing current pulses or externally applied shocks. The rate of rise of the slow response was determined by electrical or numerical differentiation and could be compared with measurements of peak inward current from the same preparation.

The three-micro-electrode method is susceptible to errors due to imperfect sealing at the impalement sites (Adrian *et al.* 1970; Schneider & Chandler, 1976). Leaky impalements are of special concern in a multicellular tissue like cardiac muscle since damaged cells tend to uncouple

TABLE 1. Composition of solutions

	Na	Mg	Tris	K	Ca	Sr	Cl	TTX
				mM				μM
A	150	0·5	10*	4	5·4	—	155·8	—
B	150	0·5	10*	16	5·4	—	167·8	3
C	150	0·5	10†	4	—	5·4	173·0	10

* Tris-maleate (titrated with ~ 10 mM-NaOH).
† Tris base- Tris HCl.
All solutions pH 7·2–7·4.

from their neighbours. Impalement leaks and uncoupling both promote attenuated measurements of the true membrane potential in the bulk of the cable. Such errors in the V_1 or V_2 signals produce an artifactual component on ΔV. This shows up during voltage clamp pulses as a positive or negative pedestal on the ΔV record which cannot be seen on I_T. We were able to avoid such problems by using relatively fine electrodes and by rejecting V_1 or V_2 impalements with unsatisfactory common-mode rejection ratio during stimulated action potentials.

THEORY

This section gives a theoretical rationale for simultaneous recordings of ΔV and I_T during the study of regenerative inward currents. According to the theory, quantitative agreement between ΔV and I_T provides an indication of their validity as measurements of current density in the face of longitudinal non-uniformity. Questions of radial non-uniformity are treated later (p. 217). Our approach is an extension of the three-micro-electrode method developed by Adrian *et al.* (1970) for skeletal muscle (see also Schneider & Chandler, 1976). Fig. 1*A* shows the electrode arrangement in the skeletal muscle experiments. The end of the fibre is at $x = 0$; voltage recording electrodes (V_1, V_2) impale the fibre at $x = l$ and $x = 2l$ respectively. Current passed by a third intracellular electrode (I_T) is used to control V_1. The method capitalizes on the fact that transmembrane current near the end of the fibre must be supplied by longitudinal current flow from the current source. The longitudinal currents produce an IR drop in the fibre's internal resistance, which is measured as a voltage difference, $V_2 - V_1 \equiv \Delta V$. Using linear cable theory, Adrian *et al.* showed that the membrane current per unit fibre length at V_1 is well approximated by the equation

$$i_m \doteqdot \frac{2}{3l^2 r_i} \Delta V, \tag{1}$$

where r_i is the internal resistance per unit length of fibre.

The approach illustrated in Fig. 1*A* has been very useful in the study of non-regenerative currents in skeletal muscle. However, as Adrian *et al.* point out, the method also has drawbacks. The total applied current is not generally interpretable because of unequal current flow into the short and long ends of the muscle fibre. If the membrane characteristic is regenerative, the technique becomes less satisfactory. All-or-nothing responses may arise in the long end of the fibre and produce artifacts in the ΔV record (see fig. 8 of Adrian *et al.* 1970). Also, the approximation in eqn. (1) is much less valid for negative conductance than for positive conductance.

Fig. 1*B* shows how these problems were circumvented in adapting the ΔV method for regenerative inward currents. The accuracy of ΔV for negative membrane conductance was improved significantly by using equal electrode spacings. Considerations of optimum spacing are given below. Escaped action potentials were avoided by using shortened Purkinje fibre bundles (Deck, Kern & Trautwein, 1964; Hecht, Hutter & Lywood, 1964). Like some other cardiac preparations, Purkinje fibres can be reduced to an effective length which is appropriate to the longitudinal space constant during the flow of slow inward current. Problems of interpretation of the total applied current are also easily avoided, in contrast to the situation in Fig. 1*A*. In the short fibre, the current-passing electrode can be positioned midway between the sealed ends so that current flows symmetrically into each hemicable. Thus, total current can be interpreted as in the conventional two-micro-electrode method of Deck *et al.* (1964). Together I_T and ΔV provide independent but simultaneous measurements of membrane current density.

Effect of interelectrode spacings

The accuracy of ΔV is strongly dependent on the spacings l and αl as defined in Fig. 1*B*. The effect of these spacings can be analysed with the help of the lumped equivalent circuit. The aim is to measure i_m, the membrane current density per unit length at V_1, the point of voltage control. The ΔV signal is generated by the ohmic drop across the resistance between V_2 and V_1, $\alpha l r_1$. The longitudinal current along this resistance varies continuously, but a representative value is the current midway between V_2 and V_1 (dashed line). This longitudinal current is equal to the total trans-membrane current between the dashed line and the end of the fibre, approximately $i_m\, l(1+\alpha/2)$, represented by the shaded element. From Ohm's law,

$$i_m\, l(1+\alpha/2) \doteqdot \frac{\Delta V}{\alpha l r_1}. \tag{1}$$

Solving for i_m,

$$i_m \doteqdot \frac{1}{\alpha(1+\alpha/2)\, l^2 r_1}\Delta V. \tag{2}$$

This expression can be made exact by introducing a correction factor p as in the treatment of Adrian *et al.* (1970).

$$i_m = p\frac{1}{\alpha(1+\alpha/2)\, l^2 r_1}\Delta V. \tag{3}$$

The correction factor p can be expressed analytically for a linear cable. For a passive membrane ($g_m > 0$), the voltage distribution varies as $V_0 \cosh(x/\lambda)$ where $\lambda =$

$(r_1 g_m)^{-\frac{1}{2}}$. Letting $L = l/\lambda$, and noting that $i_m = g_m V_1$, eqn. (3) can be solved for p:

$$p = \alpha(1+\alpha/2)\, L^2 \left[\frac{\cosh L}{\cosh[(\alpha+1)L] - \cosh L}\right]. \quad (4)$$

The expression for p approaches unity as the membrane conductance becomes small. This is the ultimate justification for the geometrical parameters of the lumped approach given above to derive eqn. (2).

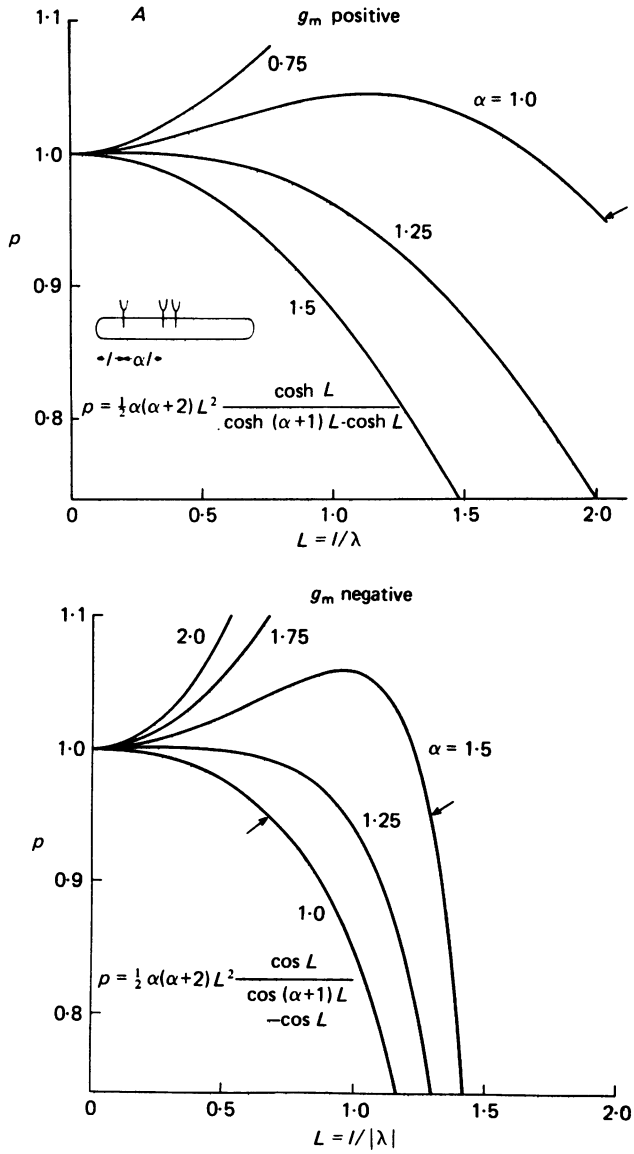

Fig. 2. Correction factor p as a function of electrode spacings. Abscissa gives electrotonic distance from V_1 to sealed end. The parameter α is the spacing ratio (inset). Arrows mark point at which p falls to 0·95. *A*, positive membrane conductance (see also Almers, 1971). *B*, Negative membrane conductance.

Fig. 2*A* plots p as a function of L for various values of α. A similar diagram has already been given by Almers (1971) but we include Fig. 2*A* for the sake of comparison with Fig. 2*B*. For regular electrode spacings ($\alpha = 1$), the graph shows the curve given by Adrian *et al.* (1970, fig. 2). In this case, the correction factor stays within 5% of unity for $L \leqslant 2$. The plot also shows that unequal spacings ($\alpha \neq 1$) give less favourable conditions for accurate measurement of i_m (Almers, 1971).

The main concern in this paper is the optimum electrode spacing for measurement of regenerative inward current. For a negative conductance ($g_m < 0$), eqn. (2) still approximates the membrane current. However, in the expression for p, cosh functions are replaced by cosines. Eqn. (4) then becomes

$$p = \alpha(1+\alpha/2)\, L^2 \frac{\cos L}{\cos[(\alpha+1)\, L] - \cos L}, \tag{5}$$

where in this case $L = l/|\lambda|$ and $|\lambda| = (-g_m r_i)^{\frac{1}{2}}$. This expression for p is plotted for various values of α in Fig. 2*B*. Here, when $\alpha = 1$, the error exceeds 5% as soon as $l > 0{\cdot}65\ |\lambda|$ (Adrian *et al.* 1970).

Fig. 2*B* also shows results with irregular electrode spacings ($\alpha \neq 1$). Surprisingly enough, unequal spacings increase the range over which the ΔV method faithfully reflects membrane current. For $\alpha = 1{\cdot}5$, the correction factor p remains within 6% of unity for $l < 1{\cdot}3\ |\lambda|$. This is a significant improvement: a doubling of the permitted value of $l/|\lambda|$ is equivalent to a fourfold increase in the range of currents which can be adequately measured.

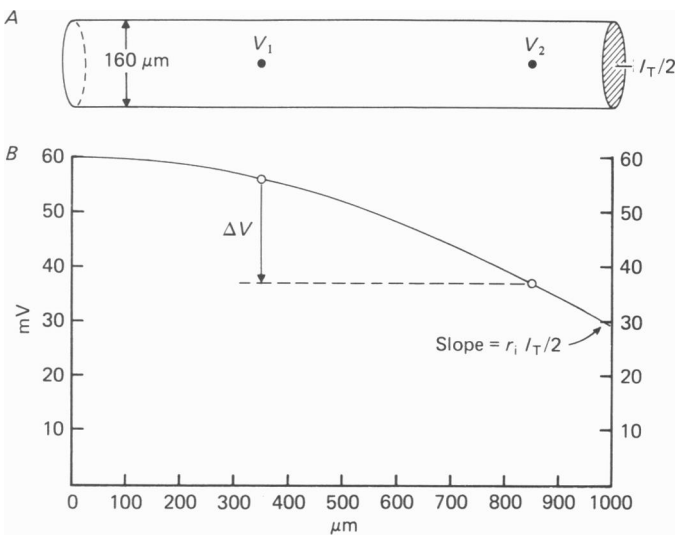

Fig. 3. Cable calculations illustrating the relation between I_T, ΔV, and an assumed membrane characteristic. *A*, cable geometry and electrode spacings. *B*, example of a voltage profile with $R_i = 200\ \Omega$ cm, the membrane I–V relation shown as the continuous curve in *C* or *D*, and a starting voltage of $V = +60$ mV. The evaluation of ΔV and I_T is indicated. Abscissa gives distance from sealed end (also for panel *A*). *C*, theoretical I–V relation compared with ΔV and I_T, determined as in *B* (see text). Smooth curve given by eqns. (7) and (8) with $G_c = 0{\cdot}5$ mmho/cm², $\bar{G} = 2{\cdot}0$ mmho/cm²,

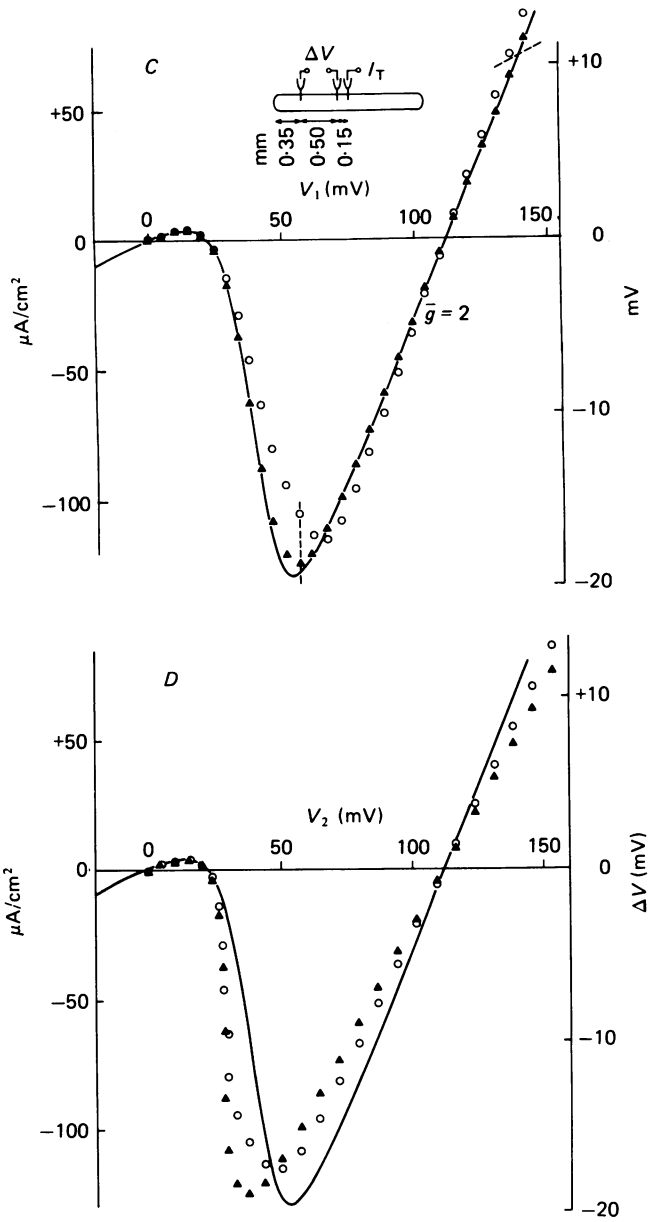

$\hat{V}_{rev}$ = 140 mV, V_y = 40 mV and k = 6 mV. Values of ΔV and I_T are represented as current density and are plotted against V_1. Vertical dashed line is drawn at a potential where ΔV is most negative ($\hat{V}_1$). *D*, same set of calculations as in *C* but with ΔV and I_T plotted against V_2. Membrane current: ——, actual; ▲, ΔV; ○, I_T.

Cable calculations for non-linear membrane

Considerations of linear membrane characteristics are convenient because the correction factor p can be expressed in closed analytical form. The next step was to explore the faithfulness of ΔV in reporting non-linear membrane characteristics of the type encountered experimentally. Cable calculations illustrated in Fig. 3 are based on a simplified membrane I–V characteristic with a leak conductance (G_0) and a regenerative inward current. The inward current had a maximal conductance $\bar{G}$ and was gated by y_∞, a voltage-dependent activation variable. The membrane current density in μA/cm^2 cylindrical fibre surface was given by

$$I_m = G_0 V + \bar{G}(V - V_{rev})\, y_\infty, \tag{6}$$

$$y_\infty = [1 + \exp(-V - \bar{V})/k)]^{-1}. \tag{7}$$

An example of this non-linear I–V relation is plotted as the continuous curve in Fig. 3*C* or 3*D* (see Figure caption for parameter values). In this case, the maximal inward current of roughly 120 μA/cm^2 was larger than that expected for the slow inward current (see Results).

Next, the I–V relation was combined with a cable geometry appropriate to the experiments (Fig. 3*A*). In the model, fibre radius $a = 80\,\mu$m, axial resistivity $R_i = 200\,\Omega$ cm, $l = 350\,\mu$m and $\alpha l = 500\,\mu$m. The voltage distribution along the length of the cable was then obtained by integration of the cable equation

$$\frac{d^2V}{dx^2} = r_i\, i_m = \frac{2R_i}{a} I_m. \tag{8}$$

Numerical integration was carried out with the modified Euler technique (Gerald, 1970), starting with an assigned value for V at $x = 0$, and the sealed end boundary condition, $(dV/dx)_{x=0} = 0$. Fig. 3*B* illustrates the results for a particular voltage profile which was started at $V(x = 0) = +60$ mV. The open circles show calculated values of V_1 and V_2 at the appropriate positions along the cable. The difference $V_2 - V_1 = \Delta V = -19$ mV. The slope of the voltage profile at $x = h$ is used to evaluate $I_T/2$, the axial current flowing into the hemicable:

$$I_T/2 = (-i_a)_{x=h} = \frac{1}{r_i}\left(\frac{dV}{dx}\right)_{x=h}. \tag{9}$$

In this example, $I_T = 1{\cdot}08\,\mu$A.

The voltage profile calculation in Fig. 3*B* simulates 'measurements' of ΔV and I_T for one particular value of V_1. To simulate 'measurements' over a wide range of V_1, similar calculations were carried out for a series of different starting values of $V(x = 0)$. The results are plotted as simulations of experimental I–V_1 curves in Fig. 3*C*. Both I_T and ΔV are normalized with respect to cable geometry: the total current is plotted as

$$I_T/\text{apparent cylindrical area} = I_T/4\pi ah. \tag{10}$$

The voltage difference signal is directly calibrated by the right hand vertical scale. The conversion between the right and left scales is obtained from eqn. (3):

$$(I_m)_{\Delta V} = \frac{(i_m)_{\Delta V}}{2\pi a} = \frac{1}{2\pi a} \cdot \frac{1}{\alpha(1+\alpha/2)\, l^2 r_i} \Delta V = \frac{a}{2\alpha(1+\alpha/2)\, l^2 R_i} \Delta V. \quad (11)$$

Fig. 3*C* shows that the current density at the V_1 electrode is reported rather faithfully by both ΔV and I_T signals; ΔV is clearly more accurate in regions where the inward current density is largest. This simulates the experimental situation where V_1 is the signal controlled by the voltage clamp. Fig. 3*D* shows that quite different results are obtained if the same set of ΔV and I_T 'measurements' are plotted as a function of V_2, thus simulating an experiment where V_2 is chosen as the point of voltage control. In this case, both ΔV and I_T deviate significantly from the theoretical current density at V_2. Both signals exaggerate the steepness of the voltage dependent gating of inward current in a manner discussed in earlier papers (Johnson & Lieberman, 1971; Jack, Noble & Tsien, 1975; Noble, 1975). The form of the distortion is not surprising if one considers that ΔV and I_T report some sort of 'average' current density, while V_2 samples the voltage profile near one extreme. In the remainder of this paper, V_1 is taken as the signal under voltage control, although it is recognized that control of V_2 might be favoured under other circumstances.

Relative accuracy of ΔV and I_T as inward current increases

The results in Fig. 3 were obtained for a fixed membrane characteristic (eqn. (6)). $\bar{G}$ was chosen to give a maximal inward current of 120 μA/cm^2, a value larger than that expected for the slow inward current. Next, we extended these calculations over a wide range of peak inward currents by varying $\bar{G}$. As an indication of the accuracy

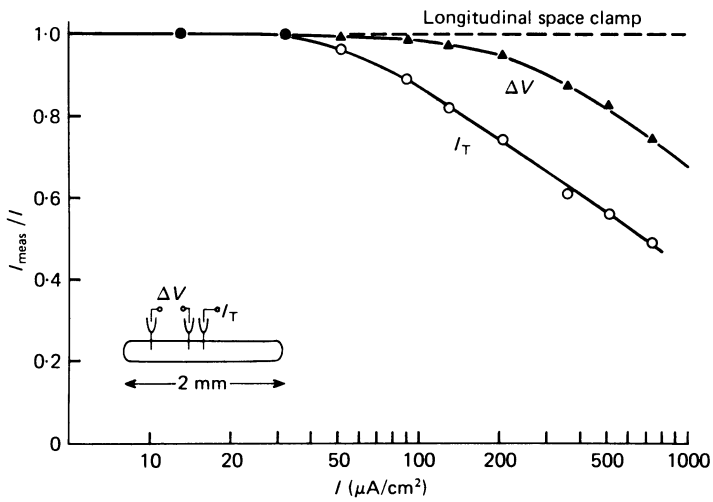

Fig. 4. Accuracy of ΔV and I_T as a function of inward current density. Ordinate plots I_{meas}, the current density 'measured' by ΔV or I_T, divided by I, the 'genuine' value of membrane current. ΔV, I_T and I are each evaluated at $\hat{V}_1$, as defined in Fig. 3. A quotient of unity for all I (dashed line) corresponds to the ideal case of a longitudinal space clamp.

of either ΔV or I_T, we compared these 'experimental' measurements with the genuine membrane current. The comparison was carried out at a potential, $\hat{V}_1$, defined for each I–V curve by the negative peak of the computed ΔV *vs.* V_1 curve (see vertical dashed line in Fig. 3*C*). This procedure seemed reasonable since $\hat{V}_1$ can be unambiguously defined in real experiments, but remains close to the voltage where the 'genuine' current is most inward in the simulations.

Fig. 4 shows the ratio between 'measured' current and 'genuine' current as the peak inward current and $\bar{G}$ are varied. If the experimental indices were ideal, the ratio would remain at unity as indicated by the dashed line ('longitudinal space clamp'). The symbols show that the ΔV and I_T signals fall off from the ideal as the regenerative inward current increases; both indices tend to underestimate the actual membrane current density. Several additional points may be illustrated by the Figure. First, I_T is quite accurate for peak currents of up to 50 μA/cm^2 cylindrical fibre surface. This is somewhat reassuring for previous experiments using the two-microelectrode method of Deck *et al.* However, the relevance of the present calculations depends on the actual electrical length of the preparation and the location of the voltage-measuring electrode. Secondly, ΔV is always a better measure of current density than I_T. Thirdly, agreement between I_T and ΔV only occurs when both signals are close to the ideal longitudinal space clamp. This qualitative conclusion would remain unaltered if the assumptions about cable geometry or axial resistivity (Fig. 3*A*) were varied. It is an important result from the experimental point of view because it provides an empirical criterion which should be satisfied by valid voltage clamp data.

ΔV *and* I_T *as measures of time-dependent current*

The preceding results were obtained for a theoretical fibre with time-independent membrane characteristics. It is to be expected that the same conclusions apply to the case of a time-dependent current if it shuts off slowly compared to the rate of longitudinal charge redistribution. This point was substantiated by the simulation of a voltage clamp experiment in a cable with capacitance and phasic inward ionic current. Starting with eqn. (8) membrane current was described as follows:

$$I_m = C_m \frac{dV}{dt} + G_o V + \bar{G}(V - V_{rev})\, df, \tag{12}$$

d was taken as a Hodgkin-Huxley type variable whose rate coefficients α_d and β_d vary exponentially with voltage.

$$\frac{dd}{dt} = \alpha_d(1-d) - \beta_d(d), \tag{13}$$

$$\alpha_d = \tau_{do}^{-1} \exp[V - \bar{V}_d)/k]; \quad \beta_d = \tau_{do}^{-1} \exp[-(V - \bar{V}_d)/k]. \tag{14}$$

In the steady state, d has the same voltage dependence as y_∞ in eqn. (6). The inactivation variable f was treated as a decaying exponential with a fixed time constant, τ_f. Following a step depolarization,

$$f = \exp -(t/\tau_f). \tag{15}$$

This simplification seemed reasonable for the slow inward current since the time

course of its inactivation is slow compared to the settling time of the membrane potential (see Fig. 6).

The voltage clamp was described by the equation

$$I_T = g_{clamp}(V_c - V_1), \tag{16}$$

where g_{clamp} was set at 0·25 mmho to represent an open loop gain of 2500 divided by a current electrode resistance of 10 MΩ. Step changes in the command potential V_c were lagged with an exponential time constant of 1 msec. These parameters were chosen so that the time course at V_1 was in reasonable agreement with the experiment. Combining eqns. (8), (12)–(16) gives the full partial differential equation. Using the same sealed end boundary condition, cable geometry and electrode placements as in Fig. 3, the equation was solved numerically by the method of Cooley & Dodge (1966).

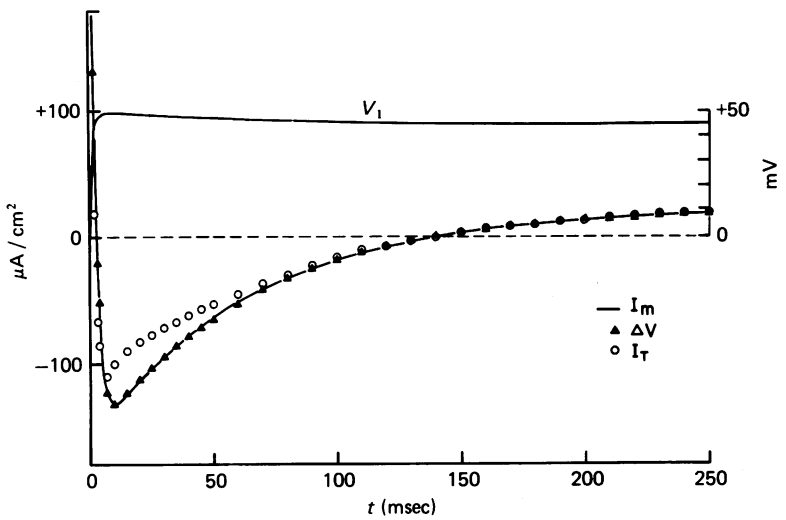

Fig. 5. Comparison between time-dependent behaviour of I_T, ΔV and I_m during a simulated voltage clamp. At $t = 0$, the command voltage was stepped from 0 mV ('resting potential') to +45 mV. The smooth curve shows I_m at V_1, where $I_m = C_m(dV_1/dt) + I_{ionic}(t, V_1)$. The peak of the early capacitative surge is off scale. $R_1 = 200\ \Omega$ cm, $C_m = 7\ \mu$F/cm², $G_o = 0{\cdot}5$ mmho/cm², $G = 2{\cdot}5$ mmho/cm², $V = 40$ mV, $k = 6$ mV, $\tau_{do} = 3$ msec, $\tau_t = 70$ msec, $V_{rev} = 140$ mV.

Fig. 5 compares I_m with I_T and ΔV for the time-dependent case. I_m is the genuine membrane current density at V_1, while I_T and ΔV are the 'experimental' measures, normalized for membrane area by eqns. (10) and (11). The upper trace gives the voltage signal V_1 associated with a 45 mV step in command potential V_c. It is evident that ΔV provides an accurate measure of I_m at all times during the clamp step. The peak inward value of I_T falls somewhat short of the peak I_m, as in the time-independent calculations (Figs. 3*C*, 4). There is also a discrepancy in time course, with I_T peaking too early relative to I_m. These shortcomings of I_T are illustrated for a membrane current density (132 μA/cm²) considerably larger than that expected for the slow inward current. For a more realistic peak I_m (~ 40 μA/cm²), similar calculations show that both I_T and ΔV are accurate in time course as well as peak value.

RESULTS

Quantitative comparison of ΔV and I_T

Fig. 6 illustrates experiments in which the slow inward current was measured simultaneously as I_T and ΔV. The upper traces show a series of depolarizing voltage pulses at V_1 from a holding potential of -46 mV. As the pulse amplitude increased, the inward current peak grew larger and the inward current inactivation was accelerated. It is clear that the wave form of the I_T and ΔV signals is very similar in all cases.

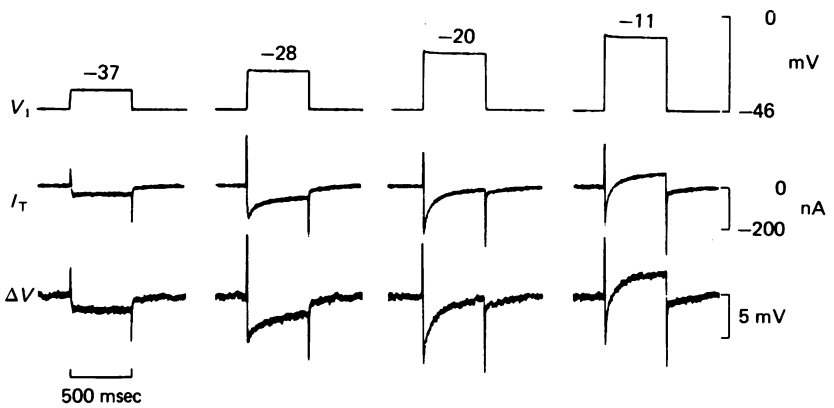

Fig. 6. Slow inward current measured by I_T and ΔV. Top traces show 500 msec voltage clamp pulses from a holding potential of -46 mV. Records of I_T (middle) and ΔV (bottom) show similar wave forms. Single records taken with chart recorder. Preparation S40-2, solution C. Bundle diameter, 144 μm; over-all length, 1800 μm; spacing l, 324 μm; spacing αl, 576 μm.

The next step was to make a quantitative comparison between I_T and ΔV. According to the theoretical results developed earlier, both signals should indicate the same membrane current density if the measurements of slow inward current are valid. A rigorous comparison between I_T and ΔV requires an independent measurement of $\alpha l r_i$, the axial resistance between V_2 and V_1 (see Fig. 1). This was done by a variety of methods in the same experiments where slow inward current was recorded. In one procedure, we followed the method used by Adrian *et al.* (1970) for skeletal muscle. The axial resistance was evaluated by applying small hyperpolarizing pulses and recording the steady deflexions in I_T and ΔV ('*DC*' case). Under these conditions, the longitudinal space constant is long relative to the electrode spacings and the approximations in the following equation (from eqn. (2)) are very good.

$$(I_T)_{DC} \doteqdot 2h(i_m)_{DC} \doteqdot \frac{2h}{\alpha(1+\alpha/2)\, l^2 r_i}(\Delta V)_{DC}. \tag{17}$$

Rearrangement gives

$$\frac{\alpha(1+\alpha/2)\, l^2 r_i}{2h} \doteqdot \frac{(\Delta V)_{DC}}{(I_T)_{DC}} \equiv R_{DC}. \tag{18}$$

This equation defines a conversion factor R_{DC} (kΩ) which can be used to convert ΔV signals into equivalent total currents.

Fig. 7*A* illustrates the determination of R_{DC} in the same experiment as in Fig. 6. I_T and ΔV were recorded during an 18 mV hyperpolarization at V_1. Several traces were signal averaged to improve the signal-to-noise ratio. In this case,

$$R_{DC} = \frac{-0{\cdot}65 \text{ mV}}{-17{\cdot}5 \text{ nA}} = 37{\cdot}0 \text{ k}\Omega.$$

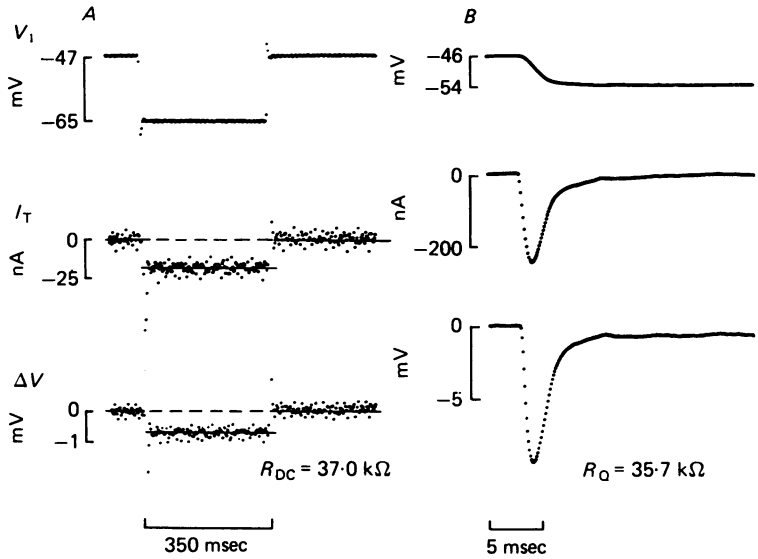

Fig. 7. The resistive scaling factor (R) determined by two methods. *A*, scaling factor R_{DC} determined from ratio of d.c. displacements of ΔV and I_T during a hyperpolarizing voltage pulse. Displacements $(\Delta V)_{DC}$ and $(I_T)_{DC}$ were measured between horizontal lines drawn through points by eye. Points are the average of twelve sweeps with a sampling interval of 3 msec. The value R_{DC} = 37·0 kΩ corresponds to R_i = 296 Ω cm. *B*, scaling factor R_Q from ratio of areas of capacitative transients, $(\Delta V)_Q$ and $(I_T)_Q$. Transient areas were obtained by numerical integration after subtraction of an ionic component with the wave form of V_1. Points are the average of twelve sweeps with a sampling interval of 0·1 msec. Preparation S40-2, total capacitance 0·08 μF, apparent cylindrical area 0·0081 cm².

This method for measuring the conversion factor R is straightforward, but is also liable to errors if imperfect sealing of the micro-electrodes leads to a false ΔV signal. Problems of measuring small signals are avoided by using the much larger transient signals associated with charging the membrane capacity. Fig. 7*B* shows capacity transients recorded during an 8·9 mV hyperpolarizing step. The areas of the transients were obtained by integration after subtracting off a very small component of ionic current with the wave form of V_1 (see fig. 3, Schneider & Chandler, 1976). The transient areas will be designated $(I_T)_Q$ (C) and $(\Delta V)_Q$ (V. sec). From cable theory (Adrian & Almers, 1974; Schneider & Chandler, 1976) it is possible to show that

$$(I_T)_Q \doteqdot 2h(i_m)_Q \doteqdot \frac{2h}{\alpha(1+\alpha/2)\, l^2 r_i}(\Delta V)_Q. \qquad (19)$$

TABLE 2. Measurements of peak inward current

Preparation	Solution	Radius (μm)	R_{DC} (kΩ)	R_Q (kΩ)	R_i (Ω cm)	Peak inward current: I_T (nA)	ΔV (mV)	$\Delta V/R_Q$ (nA)	$\frac{I_T}{\Delta V/R_Q}$
149-1	B	126	13·1	15·8	535	322	4·34	274	1·18
170-1	B	54	90·9	95·9	130	38	3·8	39·6	0·95
S40-1	C	54	—	37	300	—	—	—	—
S40-2	C	72	37·0	35·7	296	213	7·75	217	0·98
S41-2	C	72	21·7	29·7	346	—	—	—	—
S41-3	C	45	39	44	123	—	—	—	—
S43-2	C	63	20	34	224	390	8·0	333	1·17
					mean: 279				mean: 1·07

Radius of Purkinje fibre cell core was measured visually under the dissecting microscope. R_{DC} and R_Q were calculated from eqns. (18) and (20). Longitudinal resistivity was obtained as $R_i = R_Q (2\pi a^2 h)/\alpha(1+\alpha/2)l^2$.

Here $(i_m)_Q$ is the capacitative charge per unit length at V_1. The longitudinal impedance is expressed as a resistance r_i since the time constant of the longitudinal capacity, 60–70 μsec (Freygang & Trautwein, 1970) is very rapid on the time scale of the recorded transients.

As in eqn. (17), the approximations in eqn. (19) are close to exact since the *DC* space constant is long compared to the electrode spacings. Thus, eqn. (19) may be rearranged to give

$$\frac{\alpha(1+\alpha/2)\, l^2 r_i}{2h} \doteq \frac{(\Delta V)_Q}{(I_T)_Q} \equiv R_Q. \tag{20}$$

In the example given in Fig. 7*B*,

$$R_Q = \frac{25\ \mu\text{V.sec}}{0{\cdot}71\ \text{nA.sec}} = 35{\cdot}7\ \text{k}\Omega.$$

The calculations show good agreement between R_Q and R_{DC}, a typical result in the series of seven experiments (Table 2). The agreement supports the earlier assumption that the axial properties are purely resistive over a time scale slower than the capacity transient itself, although a longitudinal capacitance with a much faster time constant (Freygang & Trautwein, 1970) is certainly not excluded. R_Q may be the more reliable indicator of axial properties because it is much less susceptible to errors due to imperfect impalements. The tendency for R_{DC} to be slightly less than R_Q (Table 2) may be explained if shunt currents at the I_T or V_2 impalement sites augment $(I_T)_{DC}$.

The determinations of R in Fig. 7 allow a comparison between the I_T and ΔV signals without the use of arbitrary scaling (cf. Reuter & Scholz, 1977). Fig. 8

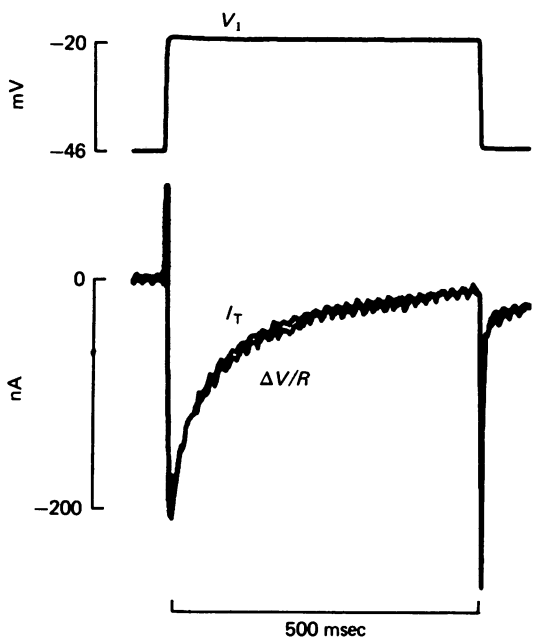

Fig. 8. Comparison between I_T and ΔV with no adjustable parameters. Records show V_1 (top) and superimposed I_T and $\Delta V/R_Q$ signals. R_Q = 35·7 kΩ, as determined in Fig. 7*B*. Traces are the average of four sweeps.

illustrates the comparison by superimposing signal averaged records of I_T and $\Delta V/R_Q$. The traces agree in magnitude as well as time course. These traces show the largest inward current peak found in this preparation. Similar agreement between I_T and $\Delta V/R_Q$ was found at other potentials. Fig. 9 shows that both indices of membrane current density give the same current–voltage relationship.

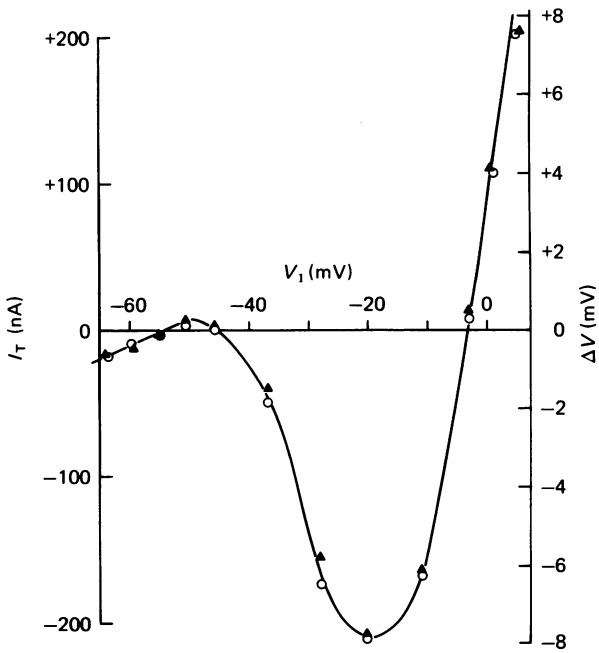

Fig. 9. *I–V* relations determined by I_T and ΔV. Peak inward current (or minimum outward current) is plotted against membrane potential V_1 for the experiment shown in Fig. 6. Right-hand ordinate refers to ΔV; left-hand ordinate refers to I_T and $\Delta V/R_Q$. Note agreement between I_T and $\Delta V/R_Q$ over the entire range of potentials.

The results in Figs. 6–9 were obtained using Sr ions as the main ionic species carrying the slow inward current. Similar correspondence between I_T and $\Delta V/R_Q$ was found when the slow inward current was supported by calcium ions (solution B, Table 2). In a total of four experiments, the ratio $I_T:(\Delta V/R_Q)$ was 1·07. The ratio seems reasonably close to unity if one considers possible sources of error. Thus the experimental results satisfy one important criterion expected theoretically for valid measurement of membrane current density.

Assessment of radial non-uniformity

Agreement between ΔV and I_T provides evidence that longitudinal non-uniformity does not seriously distort our measurements of membrane current density. However, this approach does not rule out the possibility of separate distortion due to radial non-uniformity along the narrow intercellular clefts (see Fig. 10). The membrane current density per unit length (i_m) consists of current across overt membrane (i_{surf}) in parallel with current across the mouths of the clefts (i_{clft}). The validity of

i_m as a measure of genuine properties depends upon i_{clft}, and in turn, on the absence of severe voltage drops along the cleft lumen resistance.

Unlike longitudinal non-uniformity, the radial voltage drop cannot be measured directly. However, it is possible to show that the $I-V$ relations we observed are consistent with relatively little radial non-uniformity. We calculated radial voltage

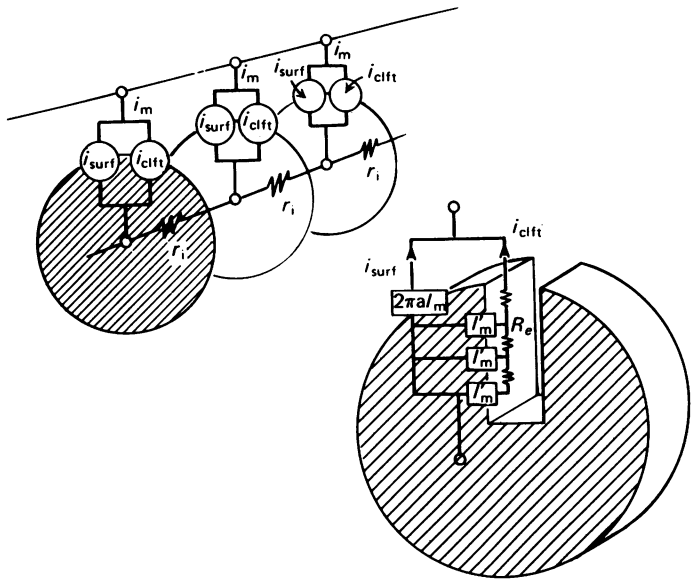

Fig. 10. Longitudinal and radial non-uniformities represented by simple equivalent circuits. *A*, membrane current per unit length (i_m) has surface (i_{surf}) and cleft components (i_{clft}) and is longitudinally distributed. *B*, more detailed representation of single disk segment from *A*. i_{clft} is the current at the input of an equivalent radial cable and will accurately reflect the genuine membrane characteristic (I'_m) if the ohmic drop along R_e is small. This treatment ignores the small effect of longitudinal current flow within the clefts, following the analysis of Hellam & Studt (1974).

profiles by taking the measured $I-V$ characteristic in Fig. 9 as a first approximation to the underlying membrane behaviour. Current amplitudes were first normalized by total membrane area, obtained from total capacitance and an assumed specific capacitance of 1 μF/cm^2. The relation between normalized current density (I'_m) and membrane potential was fitted by a smooth function (eqns. (6) and (7), continuous curve in Fig. 11*C*). The I'_m-V curve was then combined with a simplified model of the cleft geometry, shown in Fig. 11*A* (Sommer & Johnson, 1968; Hellam & Studt, 1974; Schoenberg, Dominguez & Fozzard, 1975). The model cleft is bounded by parallel membrane sheets (separation w) and filled with Tyrode solution (R_e = 50 Ω cm). The membrane characteristics are evenly distributed along the cleft membrane from the centre of the fibre (r = 0) to its outer radius (r = a). With these assumptions, the radial cable equation is like eqn. (8), but with R_e, w and I'_m in place of R_i, a and I_m. Membrane voltage V is defined as intracellular potential minus cleft lumen potential. At the centre of the fibre, the boundary condition is $(dV/dr)_{r=0} = 0$ because of radial symmetry. The cable equation was solved by numerical integration starting with various initial values of $V(r = 0)$.

Fig. 11*B* shows a radial voltage profile for a surface membrane potential that gives nearly maximal I'_m. Near the centre of the fibre the membrane is more depolarized because the lumen potential is driven negative there by centrally directed current flow. The over-all voltage span from centre to edge is only 4·4 mV in this example. Because the non-uniformity is small, the current across the cleft mouth (I_{clft}) gives a relatively good measure of I'_m. This is illustrated in Fig. 11*C*, which plots I_{clft} and

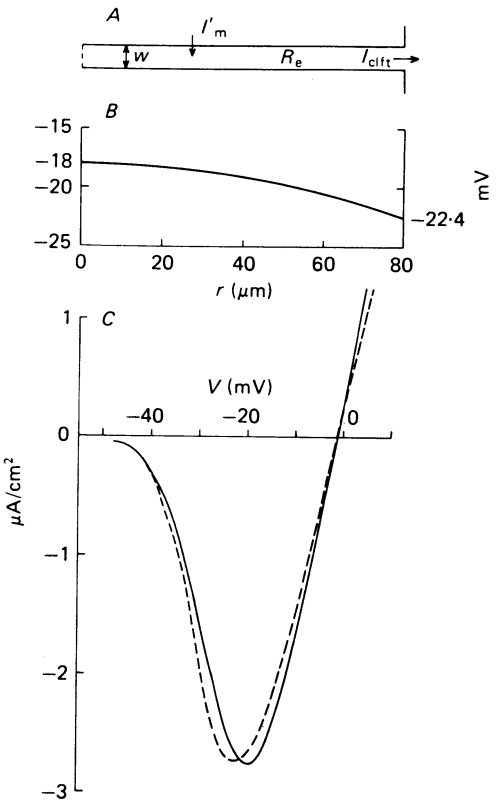

Fig. 11. Simulation of radial non-uniformity during voltage clamp experiment in Fig. 9. *A*, simplified cleft model. I_{clft} is current across mouth of radial cable after normalization for cleft membrane area. Values of R_e = 50 Ω cm and w = 200 Å were assumed. *B*, membrane voltage as a function of radial distance for near-maximal membrane current. *C*, comparison between I_{clft} (dashed) and I'_m (continuous) as functions of membrane potential at the mouth of the cleft.

I'_m as a function of surface membrane potential, $V(r = a)$. I_{clft} was obtained from $(dV/dr)_{r=a}$ for a series of profiles like Fig. 11*B*, and is normalized by cleft membrane area to allow direct comparison with I'_m. The discrepancy between I_{clft} and I'_m increases with membrane current density but, expressed in terms of a voltage displacement, it never exceeds 3 mV.

The estimated distortion is sensitive, of course, to the model parameters. For example, w was set at 200 Å in Fig. 11. The error between I'_m and I_{clft} would be decreased by taking larger values of 300 Å (Sommer & Johnson, 1968) or 400 Å (Hellam & Studt, 1974). On the other hand, the distortion would be increased by

taking a larger value for cleft length due to tortuosity (Mobley & Page, 1972). These considerations leave unchanged the basic conclusion that radial non-uniformity is not severe and current–voltage relations are not seriously distorted in the present experiments.

Comparison between measured inward current and slow response

Action potentials dependent on slow inward current could be recorded under the conditions of our experiments. The rising phase of such 'slow responses' provided another experimental check on the validity of the voltage clamp data. If radial non-uniformity is slight, measured $I-V$ characteristics may be expected to account for the slow response upstroke. On the simplest view, ionic current (i_i), membrane capacitance (c_m) and upstroke velocity should be related by the equation for a spatially uniform or 'membrane' action potential

$$-\frac{i_i}{c_m} = \frac{dV}{dt}. \tag{21}$$

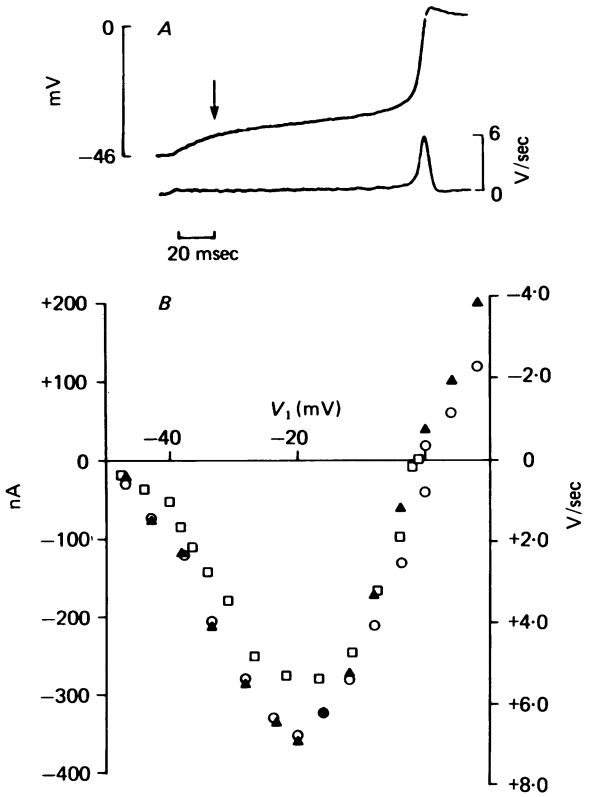

Fig. 12. Comparison of inward current using slow response and voltage-clamp measurements. *A*, slow response (top trace) elicited by termination of a −10 nA holding current. Bottom trace shows rate of rise of slow response obtained by numerical differentiation. *B*, dV/dt from panel *A* (right-hand ordinate) and peak inward current from a preceding voltage-clamp run plotted *vs.* membrane potential. Holding potential was −47 mV. Symbols give I_T, $\Delta V/R_{DC}$ and $C_T \dot{V}$ in nA (left ordinate). Scaling between right and left ordinates is appropriate to the total capacitance measured as in Fig. 7*B*. Preparation S43-2, total capacitance 0·052 μF, apparent cylindrical area 0·0057 cm^2.

This straightforward approach is possible because of various properties of the slow response and slow inward current. First, longitudinal uniformity during the response can be achieved by appropriate stimulus conditions and verified by discrete voltage impalements. Secondly, unlike the rapid I_{Na}-dependent upstroke, the slow response is sluggish compared to the 1–2 msec needed to charge cleft membrane capacity (Carmeliet & Willems, 1971; Schoenberg *et al.* (1975)). Thus, c_m can be taken as c_T, the total preparation capacitance, rather than some smaller value such as the external surface capacitance. In any event using c_m makes the comparison between i_i and (dV/dt) more stringent since severe non-uniformity would lead to underestimation of $(i_i)_{max}$ (see Noble, 1975; Schoenberg & Fozzard, 1979). Finally, the kinetics of the slow inward current are convenient for this type of analysis: activation is rapid and inactivation is slow on the time scale of the slow response. This makes it reasonable to expect that measured peak currents may approximate the net ionic current during the upstroke.

Fig. 12*A* shows the membrane potential V and its first derivative (dV/dt) during a slow response. The upstroke was initiated by a step change in applied current (arrow), from -10 to 0 nA. Voltage recording at another impalement site (not shown) established that the slow response was longitudinally uniform. The recorded upstroke is given a phase plane representation in Fig. 12*B* by plotting dV/dt against V (open squares). This plot shows that the maximum rate of rise, roughly 6 V/sec, occurs at a membrane potential near -18 mV. The left hand ordinate gives the magnitude of c_T (dV/dt) where $c_T = 0{\cdot}052\ \mu$F. The left hand scale also applies to data for I_T (open circles) and $\Delta V/R$ (triangles) from the same experiment. It is evident that the voltage clamp measurements are in rather good agreement with $c_T(dV/dt)$ over the entire range of potentials. The small discrepancy is in the wrong direction for an error due to non-uniformity. It might be explained, however, if the activation of I_{si} during the slow response falls slightly short of the peak activation during a voltage clamp step due to the kinetics of channel opening.

DISCUSSION

There is fairly general agreement on the existence and physiological importance of a slow inward current, largely carried by Ca or other divalent cations and distinct from the rapid excitatory Na current (see for example, Reuter, 1973; Cranefield, 1975). At the same time, voltage clamp experiments on the slow inward current remain controversial (see Johnson & Lieberman, 1971; Tarr & Trank, 1974; Connor *et al.* 1975; Morad & Goldman, 1976; Trautwein & McDonald, 1978). Our main purpose was to develop some criteria for valid voltage clamp results and to apply them to measurements of slow inward current. The results indicate that in calf Purkinje fibres, longitudinal and radial non-uniformities are small enough to cause relatively little distortion in measurements of peak slow inward current.

ΔV as a measure of membrane current

The voltage difference method of Adrian *et al.* (1960) is remarkable in its ability to extract useful information about membrane properties in the face of severe longitudinal non-uniformity. This feature is complemented by favourable properties of cardiac preparations in adapting the method for better measurements of regenerative

inward currents. The ΔV signal can be interpreted with less concern for effects due to three-dimensional current spread near the current-passing micro-electrode. The accuracy of ΔV can be optimized by choosing the length of the preparation and the electrode spacings to suit the ionic current of interest.

The ΔV method also has important drawbacks. It is subject to errors due to leaks around the electrode impalement sites (Adrian *et al.* 1970; Schneider & Chandler, 1976; p. 204). The most serious limitation may be the speed of voltage control, which is limited by cable delay between the point of current injection and the V_1 electrode. Switching the point of voltage control to the closer V_2 electrode improves the apparent speed but also sacrifices accuracy as discussed above. The speed of voltage control is not crucial for the present measurement of peak slow inward current because of the relatively slow time course of inactivation. However, it would be a serious obstacle to analysis of the kinetics of slow inward current activation. Such analysis might be carried out more easily using the second difference method of Adrian & Marshall (1977), which measures current density in the vicinity of the nearer voltage electrode.

Longitudinal non-uniformity

The ΔV measurements not only report membrane current density but also provide a direct measure of longitudinal non-uniformity. In Fig. 6 and other similar experiments, the largest ΔV signal was about 8 mV or less. More intense currents and more severe longitudinal non-uniformity could have been tolerated without appreciable distortion of the peak I–V relation. As Fig. 3*C* indicates, both I_T and ΔV can faithfully report i_m for ΔV signals up to 20 mV. The effectiveness of these measures depends, of course, on the choice of V_1 and not V_2 as the point of voltage control (compare panels *C* and *D* in Fig. 3). Both I_T and ΔV report a spatial average of current density over an extended region of the longitudinal cable. Since the V_1 signal is representative of the membrane potential over the same region, pairing the measured current with V_1 minimizes the distorting effects of the longitudinal cable.

Quantitative agreement between I_T and $\Delta V/R$ was very good during the flow of slow inward current (Figs. 8, 9; Table 2). This provides a direct check against longitudinal cable distortion: according to the theoretical results (Fig. 4), such agreement only occurs when both signals report membrane characteristics that would be obtained with an ideal longitudinal space clamp. Our evidence complements experiments on slow inward current in ventricular muscle by Reuter & Scholz (1977), who found good agreement between the wave forms of the ΔV and I_T signals. Their I_T was applied with a single sucrose gap, but the rationale for comparing I_T and ΔV was similar to that used in three-micro-electrode experiments (Kass & Tsien, 1975; Lederer & Tsien, 1976).

Radial non-uniformity

The next stage of analysis concerns radial non-uniformity arising from current flow along intercellular clefts. The effects of longitudinal and radial non-uniformity can be largely separated because the respective cables have a hierarchical relationship (Fig. 10). The longitudinal cable consists of a collection of disk segments (*A*), each segment containing its own equivalent radial cable (*B*). Agreement between I_T and $\Delta V/R$ indicates the longitudinal accuracy of the measurement of i_m in the disk segments, but i_m still includes the distorting effect of the radial cable.

Unlike longitudinal non-uniformity, the radial voltage drop cannot be measured by direct micro-electrode recording. One must rely on indirect arguments against serious radial cable distortion. In one approach, we estimated the radial voltage profile by combining our electrical data with a simplified structural model (Fig. 11). The calculations suggest that the voltage span from centre to surface remained less than 5 mV during the most intense slow inward current in our experiments, and that radial cable distortion was small. In another kind of check, we compared the peak $I-V$ characteristic with the slow response from the same preparation. Measurements of ionic current and upstroke velocity were quantitatively related in the manner expected for a spatially uniform action potential. Such agreement would not be expected if the ionic current were underestimated due to severe radial non-uniformity, as in the case of the excitatory sodium current (Noble, 1975; Schoenberg & Fozzard, 1979). These arguments against a serious effect of radial non-uniformity are reinforced by experiments on slow inward current in rabbit Purkinje fibres (Colatsky & Tsien, 1979). Although the clefts of these preparations are roughly thirty times wider than those of sheep or calf Purkinje fibres, the measured characteristics of the slow inward current are very similar.

Comparison between longitudinal and radial cable problems

The relative importance of radial and longitudinal non-uniformity is of general concern in the design of voltage clamp experiments. The longitudinal and radial cables are analogous in a number of respects. In the generally accepted model of Purkinje fibre structure, the radial cable is unbranched and untapered, like the longitudinal cable. Both cables have similar boundary conditions at their terminations, a current source at one end ($x = h$ or $r = a$) and zero current flow at the other end ($x = 0$, $r = 0$). Thus, the seriousness of the non-uniformity hinges on the electrical length in the longitudinal and radial directions. Let us compare (h/λ_l) against (a/λ_r) for the simplest case, where the membrane has a large resistance. The longitudinal space constant (λ_l) is given by

$$\lambda_l = \sqrt{\frac{R_m}{R_i}\frac{a}{2}}, \tag{22}$$

where R_m is the membrane resistance referred to smooth cylindrical surface. The radial space constant (λ_r) is given by

$$\lambda_r = \sqrt{\frac{R'_m}{R_e}\frac{w}{2}}, \tag{23}$$

where R'_m is the membrane resistance referred to actual membrane area. The longitudinal and radial cables are each terminated by the condition of zero current flow along the cable axis. Thus it seems appropriate to take the ratio of longitudinal electrotonic distance (h/λ_l) to radial electrotonic distance (a/λ_r) for a typical preparation:

$$\frac{h/\lambda_l}{a/\lambda_r} = \frac{h\lambda_r}{a\lambda_l} = \frac{h}{a}\sqrt{\frac{R'_m}{R_m}\frac{R_i}{R_e}\frac{w}{a}} = \frac{1000\ \mu m}{80\ \mu m}\,10\sqrt{\frac{200\ \Omega\ cm}{50\ \Omega\ cm}\cdot\frac{0{\cdot}02\ \mu m}{80\ \mu m}} = 1{\cdot}25. \tag{24}$$

The factor of 10 is the ratio of total membrane area to smooth cylindrical area (Mobley & Page, 1972). Once again, the cleft width has been taken conservatively as 200 Å rather than the more favourable value (400 Å) given by Hellam & Studt

(1974). If the assumption of uniform membrane properties is correct, this calculation suggests that the longitudinal and radial cables in a typical preparation are very similar in their effective length.

Despite this similarity, the radial non-uniformity can be expected to pose greater difficulties for the measurement of membrane properties. Membrane potential is measured at the input of the radial cable, at the mouth of the clefts, and not at a more favourable position part way toward the other termination. In this sense, the radial problem is similar to the longitudinal case when voltage control is imposed on the V_2 signal (Fig 3*D*). Radial non-uniformity would become serious in calf or sheep Purkinje fibres for conductances appreciably larger than the slow inward current. To study more intense currents, it may be necessary to use other cardiac preparations with more favourable electrical structure.

We thank Dr Thomas Colatsky and Ms Susan Wiggers for their comments on the manuscript. This work was supported by grant HL 13306 from the U.S. Public Health Service and an Established Investigatorship from the American Heart Association.

REFERENCES

ADRIAN, R. H. & ALMERS, W. (1974). Membrane capacity measurements on frog skeletal muscle in media of low ion content. *J. Physiol.* **237**, 573–605.

ADRIAN, R. H., CHANDLER, W. K. & HODGKIN, A. L. (1970). Voltage clamp experiments in striated muscle fibres. *J. Physiol.* **208**, 607–644.

ADRIAN, R. H. & MARSHALL, M. W. (1977). Sodium currents in mammalian muscle. *J. Physiol.* **268**, 223–250.

ALMERS, W. (1971). The potassium permeability of frog muscle membrane. Ph.D. Thesis, University of Rochester, Rochester, N.Y.

ATTWELL, D. & COHEN, I. (1977). The voltage clamp of multicellular preparations. *Prog. Biophys. molec. Biol.* **31**, 201–245.

CARMELIET, E. & WILLEMMS, J. (1971). The frequency dependent character of the membrane capacity in cardiac Purkinje fibres. *J. Physiol.* **213**, 85–93.

COLATSKY, T. J. & TSIEN, R. W. (1979). Electrical properties associated with wide intercellular clefts in rabbit Purkinje fibres. *J. Physiol.* **290**, 227–252.

CONNOR, J., BARR, L. & JAKOBSSON, E. (1975). Electrical characteristics of frog atrial trabeculae in the double sucrose gap. *Biophys. J.* **15**, 1047–1067.

COOLEY, J. W. & DODGE, F. A. (1966). Digital computer solutions for excitation and propagation of the nerve impulse. *Biophys. J.* **6**, 583–599.

CRANEFIELD, P. F. (1975). *The Conduction of the Cardiac Impulse.* Mount Kisco, N.Y.: Futura.

DECK, K. A., KERN, R. & TRAUTWEIN, W. (1964). Voltage clamp technique in mammalian cardiac fibres. *Pflügers Arch. ges. Physiol.* **280**, 50–62.

FOZZARD, H. A. & BEELER, G. W., JR. (1975). The voltage clamp and cardiac electrophysiology. *Circulation Res.* **37**, 403–413.

FREYGANG, W. H. & TRAUTWEIN, W. (1970). The structural implications of the linear electrical properties of cardiac Purkinje strands. *J. gen. Physiol.* **55**, 524–547.

GERALD, C. F. (1970). *Applied Numerical Analysis.* Reading, Mass.: Addison-Wesley Publishing Co., Inc.

HECHT, H. H., HUTTER, O. F. & LYWOOD, D. (1964). Voltage-current relation of short Purkinje fibres in sodium-deficient solution. *J. Physiol.* **170**, 5*P*.

HELLAM, D. C. & STUDT, J. W. (1974). A core-conductor model of the cardiac Purkinje fibre based on structural analysis. *J. Physiol.* **243**, 637–660.

JACK, J. J. B., NOBLE, D. & TSIEN, R. W. (1975). *Electric Current Flow in Excitable Cells.* Oxford: Oxford University Press.

JOHNSON, E. A. & LIEBERMAN, M. (1971). Heart: excitation and contraction. *A. Rev. Physiol.* **33**, 479–532.

KASS, R. S., SIEGELBAUM, S. A. & TSIEN, R. W. (1978). Can slow inward current be adequately voltage clamped in cardiac Purkinje fibres? *Biophys. J.* **21**, 562*a*.

KASS, R. S. & TSIEN, R. W. (1975). Analysis of the three microelectrode method as applied to inward currents in cardiac Purkinje fibres. *Biophys. J.* **15**, 257*a*.

LEDERER, W. J. & TSIEN, R. W. (1976). Transient inward current underlying arrhythmogenic effects of cardiotonic steroids in Purkinje fibres. *J. Physiol.* **263**, 73–100.

MOBLEY, B. A. & PAGE, E. (1972). The surface area of sheep cardiac Purkinje fibres. *J. Physiol.* **220**, 547–563.

MORAD, M. & GOLDMAN, Y. (1976). Clarification of membrane conductance measurements in ventricular heart muscle. *J. molec. cell. Cardiol.* **8**, 169–172.

NEW, W. & TRAUTWEIN, W. (1972). Inward membrane currents in mammalian myocardium. *Pflügers Arch.* **334**, 1–23.

NOBLE, D. (1975). *The Initiation of the Heartbeat.* Oxford: Oxford University Press.

REUTER, H. (1973). Divalent cations as charge carriers in excitable membranes. *Progr. Biophys. molec. Biol.* **26**, 1–43.

REUTER, H. (1974). Exchange of calcium ions in the mammalian myocardium. Mechanisms and functional significance. *Circulation Res.* **34**, 599–605.

REUTER, H. & SCHOLZ, H. (1977). A study of the ion selectivity and the kinetic properties of the calcium dependent slow inward current in mammalian cardiac muscle. *J. Physiol.* **264**, 17–47.

SCHNEIDER, M. F. & CHANDLER, W. K. (1976). Effects of membrane potential on the capacitance of skeletal muscle fibers. *J. gen. Physiol.* **67**, 125–163.

SCHOENBERG, M., DOMINGUEZ, G. & FOZZARD, H. A. (1975). Effect of diameter on membrane capacity and conductance of sheep cardiac Purkinje fibers. *J. gen. Physiol.* **65**, 441–458.

SCHOENBERG, M. & FOZZARD, H. A. (1979). The influence of intercellular clefts on the electrical properties of sheep cardiac Purkinje fibres. *Biophys. J.* (In the Press.)

SIEGELBAUM, S. A. (1978). Calcium-sensitive currents in cardiac Purkinje fibres. Doctoral thesis, Yale University.

SIEGELBAUM, S. A., TSIEN, R. W. & KASS, R. S. (1977). Role of intracellular calcium in the transient outward current of calf Purkinje fibres. *Nature, Lond.* **169**, 611–613.

SOMMER, J. R. & JOHNSON, E. A. (1968). Cardiac muscle. A comparative study in Purkinje fibers and ventricular fibers. *J. cell. Biol.* **36**, 497–526.

TARR, M. & TRANK, J. W. (1974). An assessment of the double sucrose-gap voltage clamp technique as applied to frog atrial muscle. *Biophys. J.* **14**, 627–643.

TRAUTWEIN, W. (1973). Membrane currents in cardiac muscle fibers. *Physiol. Rev.* **53**, 793.

TRAUTWEIN, W. & MCDONALD, T. F. (1978). Membrane conductance measurements in cat ventricular muscle. *J. molec. cell. Cardiol.* **10**, 387–394.

VEREECKE, J. & CARMELIET, E. (1971). Sr action potentials in cardiac Purkinje fibers. I. Evidence for a regenerative increase in Sr conductance. *Pflügers Arch.* **322**, 60–72.